Topological phase with a critical-type nodal line state in intermetallic CaPd

Guodong Liu, Lei Jin, Xuefang Dai, Guifeng Chen, and Xiaoming Zhang*
School of Materials Science and Engineering, Hebei University of Technology, Tianjin 300130, China

(Received 4 May 2018; published 29 August 2018)

In recent years, realizing new topological phases of matter has been a hot topic in the fields of physics and materials science. Topological semimetals and metals can conventionally be classified into two types: type-I and type-II, according to the tilting degree of the fermion cone. Here we report an unexplored topological metal phase with the critical-type nodal line between type-I and type-II nodal lines. The critical-type nodal line shows a unique nontrivial band crossing, which is composed of a flat band and a dispersive band and leads to an unexplored fermionic state. We propose intermetallic CaPd can be an existing topological metal for the fermionic state, characterized with critical-type nodal line in the bulk and drumhead band structure on the surface. Our work not only promotes the concept of a critical-type nodal line, but also provides the material realization to study its exotic properties in future experiments.

DOI: 10.1103/PhysRevB.98.075157

I. INTRODUCTION

Since the theoretical prediction and experimental confirmation of topological insulators [1–5], increasing interest in topological materials has been motivated not only by the developing requirements of fundamental physics but also by their potential technological applications. Among various topological phases, topological semimetals/metals (TMs) have become the main research focus in recent years [6–13]. TMs are characterized by symmetry-protected band crossings in the low-energy band structures. According to the dimensionality of band crossings, TMs are usually classified into three types: (1) topological nodal point semimetals/metals (TNPMs) such as Weyl and Dirac semimetals/metals [8–18], (2) topological nodal line semimetals/metals (TNLMs) [19–33], and (3) topological nodal surface semimetals/metals (TNSMs) [34–37]. Their band crossings form zero-dimensional nodal point, one-dimensional nodal line, and two-dimensional nodal surface in TNPMs, TNLMs and TNSMs, respectively. Among these TMs, TNLMs have received increasing interest. They are first predicted in several families of materials in theory [19–23,28–31,34,35], then increasing experimental confirmation has been achieved by angle-resolved photoemission spectroscopy (ARPES) [38–41]. Recently, interesting transport, magnetic, and optical properties have also been observed in TNLMs [42–45].

Depending on the slope of band dispersion in the momentum-energy space, TMs are previously termed as two types, namely type-I and type-II TMs. In type-I TMs, the bands manifest conventional conical dispersions [see Fig. 1(a)], with electron and hole regions well separated by the energy. In type-II TMs, the spectrum is completely tipped over [see Fig. 1(c)], which can give rise to the coexistence of electron and hole states at a given energy [46–49]. The physical properties of type-I and type-II TMs are drastically different [50–54]. Quite recently, the theory of the critical state between type-I and type-II TMs has also been established in Dirac/Weyl semimetals [55–57]. As shown in Fig. 1(b), the band structure of the critical-type TMs is characterized by the band crossing between a horizonal band and a dispersive band. Most importantly, the critical-type Dirac/Weyl fermions are predicted to show unique physical properties, such as Dirac/Weyl line Fermi surface, critical chiral anomaly, and unexpected topological transition under magnetic field [55–57]. For critical-type TMs, current study mostly stays at the theoretical model/concept stage, and quite rare candidate materials have been identified (except for the critical-type Dirac nodal point proposed in $Zn_2In_2S_5$ compound [57]). Especially, to date, the nodal line version of critical-type band crossing has not been proposed, and it is urgent to identify an existing material that hosts a critical-type nodal line state.

In this paper, we will fill in this research gap by identifying the critical-type nodal line state in the intermetallic material CaPd. Based on first-principles calculations, we find that there exists a closed nodal line centering X point in the $k_{x/y/z} = \pi$ plane in CaPd. Interestingly, the nodal line is formed by the crossing of a nearly flat band and a dispersive band. The unique slope of band crossing identified here is drastically different from conventional type-I and type-II nodal lines in previous examples and is considered as a critical-type nodal line state, which is possible to produce new fermions. As a clear signature of nodal line materials, the drumhead surface state is observed in CaPd. We also find that the formation of the critical-type nodal line is extremely material-specific and the candidate material is quite scarce. Our work not only proposes the concept of a critical-type nodal line state in theory, but also provides an existing material to study its properties in the future.

II. METHODS

The first-principles calculations were performed in the framework of density functional theory (DFT) by using the

*zhangxiaoming87@hebut.edu.cn

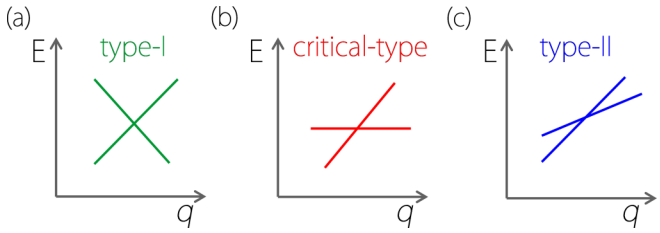

FIG. 1. Schematic figure of (a) type-I, (b) critical-type, and (c) type-II band dispersions in the momentum-energy space.

Vienna Ab initio Simulation Package (VASP) [58,59]. For ionic potentials, we used the generalized gradient approximation (GGA) of the Perdew-Burke-Ernzerhof method [60]. The cutoff energy was adopted as 500 eV, and the Brillouin zone (BZ) was sampled with Γ-centered k mesh of $15 \times 15 \times 15$ for both structural optimization and self-consistent calculations. The energy convergence criteria was chosen as 10^{-7} eV. The surface states were studied by using the software WANNIER-TOOLS [61], based on the method of maximally localized Wannier functions [62,63].

III. RESULTS AND DISCUSSIONS

Intermetallic CaPd is an existing material, first prepared by Mendelsohn *et al.* in 1973 [64]. The preparation of CaPd follows two processes: (1) pressing a 5:3 mixture of pure calcium and palladium into a pellet and (2) heating the pellet at ∼900°C for 12 h in the argon atmosphere. Later on, Iandelli *et al.* [65] and Hawanga *et al.* [66] have also synthesized high-quality crystal samples of CaPd by using a similar method. The x-ray results indicate that CaPd has a cubic structure with the CsCl-ordered crystal type. As shown in Fig. 2(a), in the unit cell, Ca and Pd atoms occupy *1a* (0, 0, 0) and *1b* (0.5, 0.5, 0.5) Wyckoff sites, respectively. The optimized lattice constant yields to be 3.534 Å, in good accordance with the experimental one (3.518 Å) [65,66].

The electronic band structure of intermetallic CaPd without spin-orbit coupling (w/o SOC) is shown in Fig. 2(c). It exhibits a metallic band structure, and near the Fermi energy the bands form two crossing points: crossing-A on the X-R path and crossing-B on the X-M path. Quite interestingly, the two crossing points are composed of a nearly flat band and a dispersive band, making both crossing-A and crossing-B critical-type nodal points.

Noticing the CaPd system reserves both time reversal (T) and spatial inversion (P) symmetries, crossing-A and crossing-B cannot be isolate nodal points but belong to the nodal line or other nodal structures, because under the protection of P and T symmetries the spinless Hamiltonian is always real valued [19]. To verify this, we first calculate the isoenergy surfaces by setting the energy level near the band crossing points (−0.38 eV). As shown in Fig. 2(d), we find the isoenergy surfaces are formed by two hole pockets which cross with each other. The crossing boundary between the hole pockets clearly manifests a closed loop in the $k_{x/y/z} = \pi$ plane, as shown by the arrows in Fig. 2(d). This indicates crossing-A and crossing-B most likely belong to a nodal line in the $k_{x/y/z} = \pi$ plane. So we make a careful investigation to band structure

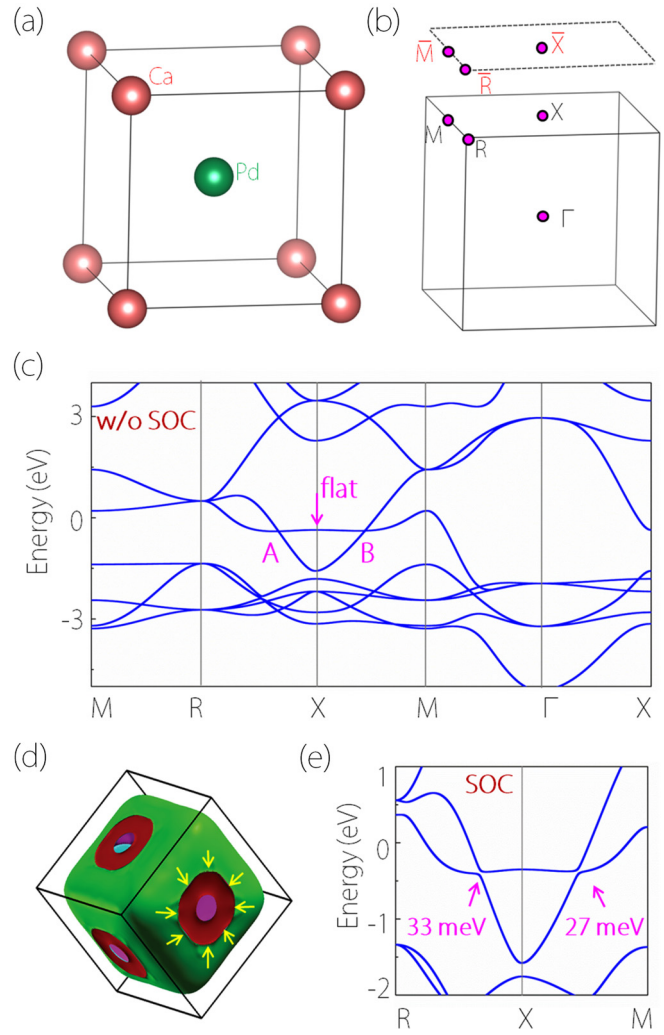

FIG. 2. (a) Crystal structure of intermetallic CaPd. (b) The bulk and surface Brillouin zone with high-symmetry points labeled. (c) Electronic band structure of CaPd along high-symmetry lines without considering SOC. (d) Isoenergy surface of CaPd at $E = E_F - 0.38$ eV. The crossing boundary between the two hole pockets is pointed by the yellow arrows. (e) Electronic band structure of CaPd along R-X and X-M paths with considering SOC. The sizes of SOC-induced gaps are indicated in the figure.

in the $k_z = \pi$ plane. As shown in Fig. 3(a), crossing-A and crossing-B indeed reside on a nodal line, which centers X point in the $k_z = \pi$ plane. Because of the cubic symmetries, there also possess nodal line in the equivalent $k_x = \pi$ and $k_y = \pi$ plane. In fact, the nodal line is constrained to lie in the $k_{x/y/z} = \pi$ plane by the mirror symmetry $M_{x,y,z}$. The nodal line locates in the mirror-invariant plane, and it also enjoys the protection of $M_{x,y,z}$, as the two crossing bands possess opposite $M_{x,y,z}$-eigenvalues.

When SOC is absent, the nodal line in CaPd is stabilized by the coexistence of P and T symmetries in the system. Similar to most nodal line materials, SOC will gap the nodal line in CaPd. As shown in Fig. 2(e), our results indicate that in CaPd the SOC-induced gaps at crossing-A and crossing-B are ∼30 meV, which are comparable or smaller than those in typical nodal line materials, such as ZrSiS (>20 meV) [39], TiB_2 (>25 meV)

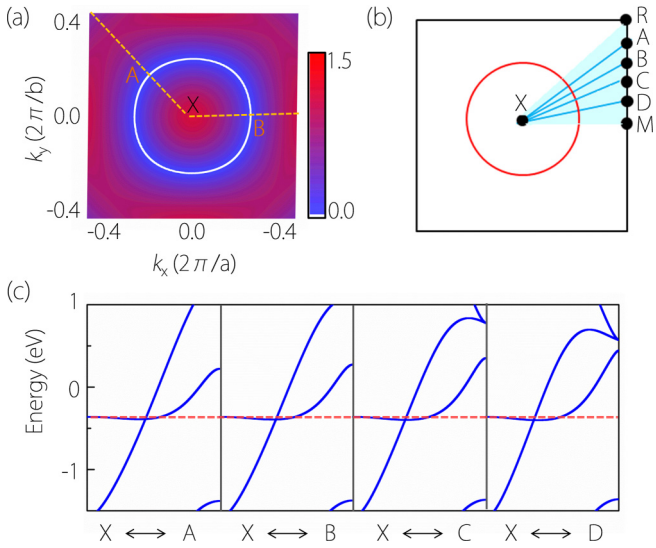

FIG. 3. (a) The shape of nodal line in the $k_z = \pi$ plane. The positions of crossing-A and crossing-B are indicated in the figure. (b) The selected k paths (X-A, X-B, X-C and X-D) through the nodal line. The points A, B, C, and D are equally spaced between M and R. (c) Electronic band structures of CaPd along X-A, X-B, X-C, and X-D paths. In (c), the horizontal dashed line serves as a guide of eye.

[28], Mg_3Bi_2 (>36 meV) [30], Cu_3NPd (>60 meV) [22,23], CaAgBi (>80 meV) [67], and so on. Considering the nodal line materials with similar size of SOC-induced gaps, including ZrSiS [39,40,42], TiB_2 [68], and Mg_3Bi_2 [69], have been experimentally verified, the nodal line signature in CaPd is also promising to be detected in experiments.

As shown in Fig. 2(c), on the nodal line, crossing-A and crossing-B manifest critical-type band crossing. Here we make further investigation to the band crossing on other parts of the nodal line. Noticing both fourfold rotation C_4 symmetry and mirror M_z symmetry preserve in the $k_z = \pi$ plane, 1/8 part of the first BZ can reflect the nature of the whole. Besides the X-M and X-R paths, we have selected four paths in the region, namely X-A, X-B, X-C, and X-D [see Fig. 3(b)]. The band structures on the four paths are shown in Fig. 3(c). We find that all the paths possess nearly critical-type band crossings, indicating the truth of critical-type signature on the whole nodal line.

It is worth noticing that the concept of critical-type nodal line state has been rarely reported. Considering that critical-type Dirac/Weyl points show different topological properties (such as critical chiral anomaly and interesting topological transition under magnetic field) with traditional type-I and type-II nodal points, critical-type nodal lines are also expected to possess these unique characteristics, because each point on the nodal line can be viewed as a critical-type nodal point in the transverse dimensions perpendicular to the line. Moreover, a critical-type nodal line should also possess distinct properties with critical-type nodal points because of their diverse dimensionality of band crossing. Such distinct properties are quite promising to be identified from transport experiments. One observation is the phase shift of the Shubnikov-de Haas oscillation. For example, previous transport studies on the nodal line material ZrSiS found that the phase shift in the

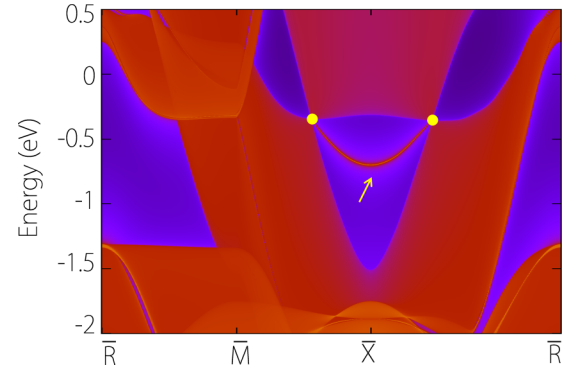

FIG. 4. (a) Projected spectrum for the Ca-terminated (001) surface of intermetallic CaPd. The yellow dots mark the position of projected bulk band-crossing points, and the yellow arrow indicates the drumhead surface states.

higher frequency component can diverse from 0 to $\pm 1/8$ under different conditions [70,71], being different from the fixed phase shift in a given Dirac/Weyl material. Especially, based on the general rule by Li *et al.* [72] established quite recently, the phase shifts of quantum oscillations in nodal line materials can show rich results depending on the magnetic field directions, carrier types, and configurations of the Fermi surface, quite different from those from normal electrons and Dirac/Weyl fermions. For the proposed critical-type nodal line, it is promising to observe both features of critical-type nodal points (such as the critical chiral anomaly) and of nodal lines (such as rich phase shifts of quantum oscillations from their nontrivial Berry phases).

One of the most representative signatures of a nodal line state is the existence of drumhead surface states [19]. For intermetallic CaPd, we show the Ca-terminated (001) surface spectrum in Fig. 4. Like type-I and type-II nodal lines, we find critical-type nodal line also manifests drumhead surface state emanated from the bulk nodal points, as pointed by the yellow arrow in Fig. 4. Because of the absence of particle-hole symmetry, the surface band is not perfectly flat but possesses an energy dispersion of about 300 meV. Similar dispersive surface states are also observed in other nodal line materials [19–22]. The existence of drumhead surface states in CaPd can be readily detected by surface-sensitive probes such as ARPES and scanning tunneling microscopy.

Finally, to further understand the nature of the nodal line state in CaPd, we construct a low-energy effective Hamiltonian at X point. The symmetry analysis indicates the two bands belong to irreducible representations A_{1g} and A_{2u} of the D_{4h} symmetry, respectively. Using them as basis states, the 2×2 effective Hamiltonian up to the quadratic order can be described as

$$\mathcal{H} = \begin{bmatrix} h_{11} & h_{12} \\ h_{21} & h_{22} \end{bmatrix}, \tag{1}$$

with

$$h_{ii} = A_i\left(k_x^2 + k_y^2\right) + B_i k_z^2 + M_i, \tag{2}$$

$$h_{12} = -h_{21} = iCk_z. \tag{3}$$

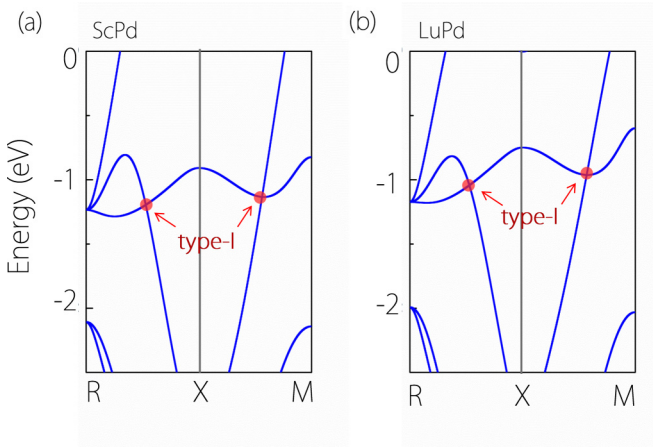

FIG. 5. Electronic band structures along the R-X and X-M paths for (a) ScPd and (b) LuPd. The crossing points in (a) and (b) show type-I band dispersion.

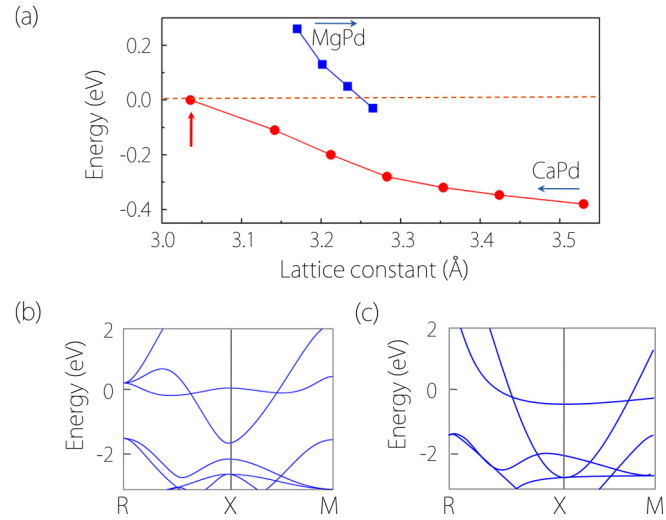

FIG. 6. (a) The position of nodal line under different lattice constants for CaPd (red line) and MgPd (blue line). (b) Band structure of CaPd under 14% lattice compression (at 3.03 Å). (c) Band structure of CaPd under 75% Mg doping ($Ca_{0.25}Mg_{0.75}Pd$).

From the Hamiltonian, we find the nondiagonal terms will vanish when $k_z = 0$ (notice, here the wave vector k is expanded from X point). This indicates that the band-crossing in the $k_{x/y/z} = \pi$ plane will produce a nodal line, which is consistent with the results from DFT calculations. In the Hamiltonian, A_i, B_i, M_i ($i = 1, 2$), and C are material-specific coefficients, which determine the details of band structure near X point. In CaPd, these model parameters can be obtained by fitting the DFT band structure. The fitting results yield $A_1 = 0.09\,\text{eV}\cdot\text{Å}^2$, $A_2 = 7.25\,\text{eV}\cdot\text{Å}^2$, $B_1 = 17.22\,\text{eV}\cdot\text{Å}^2$, $B_2 = -22.31\,\text{eV}\cdot\text{Å}^2$, $C = 15.17\,\text{eV}\cdot\text{Å}^2$, $M_1 = -0.28$ eV, and $M_2 = -1.46$ eV. The small value of A_1 produces the nearly nondispersive valence band around X point, which could be advantageous for achieving the critical nodal line. It should be mentioned that an extremely small A_1 and specific energy variation may lead to a possible quantum phase transition from paramagnetic to ferromagnetic induced by the electron-electron interaction, which has been well described in the critical point between type-I and type-II TNLMs by He *et al.* [73] quite recently. However, we note that for CaPd, the critical nodal line is stable, as there is no appearance of ferromagnetic order in our DFT calculations. From the Hamiltonian, we can also find that, besides the protection of specific symmetries, the formation of a critical-type nodal line is extremely material-specific. To show this point, we choose other two intermetallic compounds, namely ScPd and LuPd, as examples. Both ScPd [74] and LuPd [75] are existing materials with the same CsCl-type structure. The electronic band structures of ScPd and LuPd are shown in Figs. 5(a) and 5(b). We find that there also exist band-crossing points on the R-X and X-M paths in ScPd and LuPd. Under the same protection mechanism with CaPd, the crossing points in ScPd and LuPd also belong to nodal lines centering X point in the $k_{x/y/z} = \pi$ plane. However, the nodal lines in ScPd and LuPd possess conventional type-I band dispersion, drastically different from the critical-type nodal line state in CaPd. Such high material-dependence indicates the number of critical-type nodal line semimetals are quite limited in real materials.

Before closing, we want to point out that, in the ground state, the critical-type nodal line in CaPd does not close to the Fermi level (at -0.38 eV), which will greatly hamper its experimental identification (such as from transport experiments). Fortunately, we find the position of the nodal line in CaPd can be tuned near the Fermi level by strain and proper elemental doping, with the critical band-crossing signature nearly unaffected (see Appendix). Therefore, the proposed CaPd-based materials can serve as an excellent platform to study the properties of the critical-type nodal line state.

IV. SUMMARY

In summary, we have proposed a new topological phase with nearly critical-type nodal line state in intermetallic CaPd. The critical-type nodal line is the transition state from conventional type-I to type-II nodal lines, and is formed by the crossing of a flat band and a dispersive band in the momentum-energy space. In intermetallic CaPd, the critical-type nodal line resides on the $k_{x/y/z} = \pi$ plane, protected by both mirror symmetry and the coexistence of P and T symmetries. Clear drumhead surface state originating from critical-type nodal line is observed in CaPd, which is quite promising to be detected in experiments. We find that the existence of critical-type nodal line is quite material-specific, so the candidate material is very limited. Besides promoting the concept of critical-type nodal line, this work also provides an existing material to study the topological phase in future experiments.

ACKNOWLEDGMENTS

This work is supported by the Special Foundation for Theoretical Physics Research Program of China (No. 11747152), the Natural Science Foundation of Hebei Province (No. E2016202383), Chongqing City Funds for Distinguished Young Scientists (No. cstc2014jcyjjq50003). One of the

authors (G.L.) acknowledges the financial support from Hebei Province Program for Top Young Talents.

APPENDIX: BAND STRUCTURE OF CAPD UNDER LATTICE DISTORTION AND ELEMENTAL DOPING

We find the position of the nodal line in CaPd is quite sensitive with the lattice constants and elemental doping. Figure 6(a) shows the position of the nodal line under different lattice constants of CaPd (here, we use the energy of crossing-A, which represents the position of the nodal line). One can find that the nodal line in CaPd moves toward the Fermi level upon the lattice compression. The results show that a 14% lattice compression (at 3.03 Å) finally makes the nodal line quite near the Fermi level, and corresponding band structure is shown in Fig. 6(b). Besides CaPd, we find MgPd also shows the critical-type band crossing near the Fermi level (at 0.22 eV above the Fermi level). Similarly, the nodal line in MgPd can be tuned to the Fermi level by a ∼3% lattice expansion (at ∼3.24 Å), as shown in Fig. 6(a). Starting from CaPd and MgPd, we find that a ∼75% doping between them ($Ca_{0.25}Mg_{0.75}Pd$) can naturally give rise to a nodal line state near the Fermi level (−0.04 eV), as shown in Fig. 6(c). Importantly, the flat band in CaPd, which is crucial for the formation of a critical-type nodal line, does not change much during lattice compression and Mg-doping [see Figs. 6(b) and 6(c)]. Moreover, their is no appearance of ferromagnetic order based on our DFT calculations during the lattice comprssion and elemental doping. Therefore, the critical-type nodal line state is promising to be realized in CaPd-based materials.

[1] C. L. Kane and E. J. Mele, Phys. Rev. Lett. **95**, 146802 (2005).
[2] B. A. Bernevig, T. L. Hughes, and S.-C. Zhang, Science **314**, 1757 (2006).
[3] M. Z. Hasan and C. L. Kane, Rev. Mod. Phys. **82**, 3045 (2010).
[4] X.-L. Qi and S.-C. Zhang, Rev. Mod. Phys. **83**, 1057 (2011).
[5] Y. L. Chen, J. G. Analytis, J. H. Chu, Z. K. Liu, S. K. Mo, X. L. Qi, H. J. Zhang, D. H. Lu, X. Dai, Z. Fang *et al.*, Science **325**, 178 (2009).
[6] A. A. Burkov, Nat. Mater **15**, 1145 (2016).
[7] B. Yan and C. Felser, Annu. Rev. Condens. Matter Phys. **8**, 337 (2017).
[8] X. Wan, A. M. Turner, A. Vishwanath, and S. Y. Savrasov, Phys. Rev. B **83**, 205101 (2011).
[9] S. Murakami, New J. Phys. **9**, 356 (2007).
[10] H. Weng, C. Fang, Z. Fang, B. A. Bernevig, and X. Dai, Phys. Rev. X **5**, 011029 (2015).
[11] Z. Wang, Y. Sun, X.-Q. Chen, C. Franchini, G. Xu, H. Weng, X. Dai, and Z. Fang, Phys. Rev. B **85**, 195320 (2012).
[12] S. M. Young, S. Zaheer, J. C. Y. Teo, C. L. Kane, E. J. Mele, and A. M. Rappe, Phys. Rev. Lett. **108**, 140405 (2012).
[13] Z. Wang, H. Weng, Q. Wu, X. Dai, and Z. Fang, Phys. Rev. B **88**, 125427 (2013).
[14] S. A. Yang, H. Pan, and F. Zhang, Phys. Rev. Lett. **113**, 046401 (2014).
[15] Z. Zhu, G. W. Winkler, Q. S. Wu, J. Li, and A. A. Soluyanov, Phys. Rev. X **6**, 031003 (2016).
[16] X. Sheng, Z. Yu, R. Yu, H. Weng, and S. A. Yang, J. Phys. Chem. Lett. **8**, 3506 (2017).
[17] X.-L. Sheng and B. K. Nikolic, Phys. Rev. B **95**, 201402 (2017).
[18] X. Zhang, R. Guo, L. Jin, and X. Dai, and G. Liu, J. Mater. Chem. C **6**, 575 (2018).
[19] H. Weng, Y. Liang, Q. Xu, R. Yu, Z. Fang, X. Dai, and Y. Kawazoe, Phys. Rev. B **92**, 045108 (2015).
[20] Y. Chen, Y. Xie, S. A. Yang, H. Pan, F. Zhang, M. L. Cohen, and S. Zhang, Nano Lett. **15**, 6974 (2015).
[21] C. Fang, H. M. Weng, X. Dai, and Z. Fang, Chin. Phys. B **25**, 117106 (2016).
[22] Y. Kim, B. J. Wieder, C. L. Kane, and A. M. Rappe, Phys. Rev. Lett. **115**, 036806 (2015).
[23] R. Yu, H. Weng, Z. Fang, X. Dai, and X. Hu, Phys. Rev. Lett. **115**, 036807 (2015).
[24] C. Fang, Y. Chen, H. Y. Kee, and L. Fu, Phys. Rev. B **92**, 081201 (2015).
[25] L. S. Xie, L. M. Schoop, E. M. Seibel, Q. D. Gibson, W. Xie, and R. J. Cava, APL Mater. **3**, 083602 (2015).
[26] Y.-H. Chan, C.-K. Chiu, M. Y. Chou, and A. P. Schnyder, Phys. Rev. B **93**, 205132 (2016).
[27] R. H. Li, H. Ma, X. Cheng, S. Wang, D. Li, Z. Zhang, Y. Li, and X.-Q. Chen, Phys. Rev. Lett. **117**, 096401 (2016).
[28] X. Zhang, Z.-M. Yu, X.-L. Sheng, H. Y. Yang, and S. A. Yang, Phys. Rev. B **95**, 235116 (2017).
[29] S. Li, Z.-M. Yu, Y. Liu, S. Guan, S.-S. Wang, X. Zhang, Y. Yao, and S. A. Yang, Phys. Rev. B **96**, 081106(R) (2017).
[30] X. Zhang, L. Jin, X. Dai, and G. Liu, J. Phys. Chem. Lett. **8**, 4814 (2017).
[31] T.-T. Zhang, Z.-M. Yu, W. Guo, D. Shi, G. Zhang, and Y. Yao, J. Phys. Chem. Lett. **8**, 5792 (2017).
[32] X. Zhang, Z.-M. Yu, Y. Lu, X.-L. Sheng, H. Y. Yang, and S. A. Yang, Phys. Rev. B **97**, 125143 (2018).
[33] X. M. Zhang, L. Jin, F. X. Dai, and G. D. Liu, Appl. Phys. Lett. **112**, 122403 (2018).
[34] C. Zhong, Y. Chen, Y. Xie, S. A. Yang, M. L. Cohen, and S. B. Zhang, Nanoscale **8**, 7232 (2016).
[35] Q.-F. Liang, J. Zhou, R. Yu, Z. Wang, and H. Weng, Phys. Rev. B **93**, 085427 (2016).
[36] W. Wu, Y. Liu, S. Li, C. Zhong, Z.-M. Yu, X.-L. Sheng, and Y. X. Zhao, and S. A. Yang, Phys. Rev. B **97**, 115125 (2018).
[37] X. M. Zhang, Z.-M. Yu, Z. M. Zhu, W. K. Wu, S.-S. Wang, X.-L. Sheng, and S. A. Yang, Phys. Rev. B **97**, 235150 (2018).
[38] G. Bian, T.-R. Chang, R. Sankar, S.-Y. Xu, H. Zheng, T. Neupert, C.-K. Chiu, S.-M. Huang, G. Chang, I. Belopolski *et al.*, Nat. Commun. **7**, 10556 (2016).
[39] L. M. Schoop, M. N. Ali, C. Straber, A. Topp, A. Varykhalov, D. Marchenko, V. Duppel, S. S. P. Parkin, B. V. Lotsch, and C. R. Ast, Nat. Commun. **7**, 11696 (2016).
[40] M. Neupane, I. Belopolski, M. M. Hosen, D. S. Sanchez, R. Sankar, M. Szlawska, S.-Y. Xu, K. Dimitri, N. Dhakal, P. Maldonado *et al.*, Phys. Rev. B **93**, 201104 (2016).
[41] D. Takane, Z. Wang, S. Souma, K. Nakayama, C. X. Trang, T. Sato, T. Takahashi, and Y. Ando, Phys. Rev. B **94**, 121108 (2016).

[42] J. Hu, Z. Tang, J. Liu, X. Liu, Y. Zhu, D. Graf, K. Myhro, S. Tran, C. N. Lau, J. Wei, and Z. Mao, Phys. Rev. Lett. **117**, 016602 (2016).
[43] C.-L. Zhang, Z. Yuan, G. Bian, S.-Y. Xu, X. Zhang, M. Z. Hasan, and S. Jia, Phys. Rev. B **93**, 054520 (2016).
[44] M. X. Wang, Y. Xu, L. P. He, J. Zhang, X. C. Hong, P. L. Cai, Z. B. Wang, J. K. Dong, and S. Y. Li, Phys. Rev. B **93**, 020503 (2016).
[45] S.-Y. Guan, P.-J. Chen, M.-W. Chu, R. Sankar, F. Chou, H.-T. Jeng, C.-S. Chang, and T.-M. Chuang, Sci. Adv. **2**, e1600894 (2016).
[46] L. Lu, Z. Wang, D. Ye, L. Ran, L. Fu, J. D. Joannopoulos, and M. Soljai, Science **349**, 622 (2015).
[47] T.-R. Chang, S.-Y. Xu, G. Chang, C.-C. Lee, S.-M. Huang, B. Wang, G. Bian, H. Zheng, D. S. Sanchez, I. Belopolski *et al.*, Nat. Commun. **7**, 10639 (2016).
[48] A. A. Soluyanov, D. Gresch, Z. Wang, Q. Wu, M. Troyer, X. Dai, and B. A. Bernevig, Nature **527**, 495 (2015).
[49] T.-R. Chang, S.-Y. Xu, D. S. Sanchez, W.-F. Tsai, S.-M. Huang, G. Chang, C.-H. Hsu, G. Bian, I. Belopolski, Z.-M. Yu *et al.*, Phys. Rev. Lett. **119**, 026404 (2017).
[50] A. A. Zyuzin and R. P. Tiwari, JETP Lett. **103**, 717 (2016).
[51] M. Udagawa and E. J. Bergholtz, Phys. Rev. Lett. **117**, 086401 (2016).
[52] T. E. O'Brien, M. Diez, and C. W. J. Beenakker, Phys. Rev. Lett. **116**, 236401 (2016).
[53] M. Koshino, Phys. Rev. B **94**, 035202 (2016).
[54] Z.-M. Yu, Y. Yao, and S. A. Yang, Phys. Rev. Lett. **117**, 077202 (2016).
[55] G. E. Volovik, JETP Lett. **104**, 645 (2016).
[56] G. E. Volovik, Phys.-Usp. **61**, 89 (2018).
[57] H. Huang, K.-H. Jin, and F. Liu, arXiv:1711.07096.
[58] G. Kresse and D. Joubert, Phys. Rev. B **59**, 1758 (1999).
[59] G. Kresse and J. Hafner, Phys. Rev. B **47**, 558 (1993).
[60] J. P. Perdew, K. Burke, and M. Ernzerhof, Phys. Rev. Lett. **77**, 3865 (1996).
[61] Q. S. Wu, S. N. Zhang, H.-F. Song, M. Troyer, and A. A. Soluyanov, Comput. Phys. Commun. **224**, 405 (2018).
[62] N. Marzari and D. Vanderbilt, Phys. Rev. B **56**, 12847 (1997).
[63] A. A. Mostofi, J. R. Yates, Y.-S. Lee, I. Souza, D. Vanderbilt, and N. Marzari, Comput. Phys. Commun. **178**, 685 (2008).
[64] M. H. Mendelsohn and J. Tanaka, J. Less-Common Met. **32**, 314 (1973).
[65] A. Iandelli, G. L. Olcese, and A. J. Palenzona, J. Less-Common Met. **76**, 317 (1980).
[66] A. Palenzona and P. Manfrinetti, J. Less-Common Met. **85**, 307 (1982).
[67] A. Yamakage, Y. Yamakawa, Y. Tanaka, and Y. Okamoto, J. Phys. Soc. Jpn. **85**, 013708 (2016).
[68] Z. H. Liu, R. Lou, P. J. Guo, Q. Wang, S. S. Sun, C. H. Li, S. Thirupathaiah, A. Fedorov, D. Shen, K. Liu *et al.*, Phys. Rev. X **8**, 031044 (2018).
[69] T.-R. Chang, I. Pletikosic, T. Kong, G. Bian, A. Huang, J. Denlinger, S. K. Kushwaha, B. Sinkovic, H.-T. Jeng, T. Valla *et al.*, arXiv:1711.09167.
[70] R. Singha, A. K. Pariari, B. Satpati, and P. Mandal, Proc. Natl. Acad. Sci. USA **114**, 2468 (2017).
[71] M. N. Ali, L. M. Schoop, C. Garg, J. M. Lippmann, E. Lara, B. Lotsch, and S. S. P. Parkin, Sci. Adv. **2**, e1601742 (2016).
[72] C. Li, C. M. Wang, B. Wan, X. Wan, H.-Z. Lu, and X. C. Xie, Phys. Rev. Lett. **120**, 146602 (2018).
[73] J. He, X. Kong, W. Wang, and S.-P. Kou, New J. Phys. **20**, 053019 (2018).
[74] A. T. Aldred, Trans. Metal. Soc. AIME **224**, 1082 (1962).
[75] U. Walter and D. Wohlleben, Phys. Rev. B **35**, 3576 (1987).